

**DEVELOPMENT OF POST-PROCESSING
TECHNIQUE FOR METAL ARTEFACTS
REDUCTION IN THE PRESENCE OF
CONTRAST MEDIA IN CT IMAGING**

NUR DIANA BINTI MOHAMAD YUSOB

UNIVERSITI SAINS MALAYSIA

2018

**DEVELOPMENT OF POST-PROCESSING
TECHNIQUE FOR METAL ARTEFACTS
REDUCTION IN THE PRESENCE OF
CONTRAST MEDIA IN CT IMAGING**

by

NUR DIANA BINTI MOHAMAD YUSOB

**Thesis submitted in fulfilment of the requirements
for the Degree of
Master of Science**

July 2018

ACKNOWLEDGEMENT

First of all, I would like to express my ultimate gratitude towards Allah, The Almighty for all the countless gifts He has offered me and enable me to complete this project successfully. Also peace is upon Muhammad, His messenger of Islam.

It is a great pleasure to acknowledge my deepest thanks to my supervisor Dr. Rafidah Zainon, a senior lecturer in Oncological and Radiological Cluster ay Advanced Medical and Dental Institute, Universiti Sains Malaysia for being supportive and patiently taught and guided me throughout the project. It is a great honor to work under her supervision. I would also like to acknowledge the advice and guidance of my co-supervisors, Prof. Dato' Dr. Abd Aziz Tajuddin.

I also wish my sincere appreciation to Ms. Suzana Mat Isa, a Science Officer at Imaging Unit and all the radiographers and staffs for the kind support during my time working there. I humbly extend my thanks to my colleague, Ms. Nur Jihan Mohd Zukhi who helps me throughout this work and to all concerned people who co-operate with me in this study.

I wish to express my love and gratitude to my lovely parents, Mohamad Yusob Omar and Che Robiah Hanafi for their endless love and support, whose financial support and passionate encouragement make it possible to complete this project. My thanks are due to my siblings for their loving support. I would also like to extend my deepest gratitude to all my friends for their support and made my time here so enjoyable. I am grateful for the financial support from the Ministry of Higher Education Malaysia through Fundamental Research Grant Scheme (FRGS).

TABLE OF CONTENTS

ACKNOWLEDGEMENT	ii
TABLE OF CONTENTS.....	iii
LIST OF TABLES	viii
LIST OF FIGURES	ix
LIST OF ABBREVIATIONS	xv
ABSTRAK	xvi
ABSTRACT.....	xviii
CHAPTER 1 : INTRODUCTION TO THE THESIS	1
1.1 Objectives	1
1.1.1 The thesis objective.....	1
1.2 Clinical and technical background.....	2
1.3 Motivation of the study.....	5
1.4 Clinical significance	7
1.5 Thesis organisation	8
CHAPTER 2 : THEORY AND LITERATURE REVIEW.....	10
2.1 X-rays.....	10
2.1.1 Generation of X-rays.....	12
2.1.2 Interaction of X-ray with matter	13
2.1.3 The energy dependence of X-ray attenuation	16

2.2 Computed Tomography	18
2.2.1 Evolution of CT scanner	20
2.2.2 Basic principles of CT imaging.....	22
2.2.3 CT image formation	23
2.2.3(a) Scanning phase	23
2.2.3(b) Reconstruction phase.....	24
2.2.3(c) Digital-to-analogue phase.....	29
2.2.4 CT image quality.....	29
2.2.4(a) Image contrast.....	30
2.2.4(b) Spatial resolution.....	31
2.2.4(c) Image noise	32
2.2.4(d) Artefacts	33
2.3 Metal artefact reduction algorithm	34
2.3.1 Image segmentation	39
2.3.2 Interpolation	39
2.3.3 Image filtering.....	40
2.4 Contrast media usage	42
2.5 Phantom	43
2.6 Computed Tomography	46
2.7 CT imaging parameters.....	47
2.7.1 Slice Thickness.....	47
2.7.2 Pitch	48
2.8 Statistical analysis	49

CHAPTER 3 : MATERIALS AND METHOD.....	50
3.1 Quality assurance test of CT scanner.....	51
3.1.1 CT number accuracy	52
3.1.2 Image noise	53
3.1.3 Image uniformity.....	53
3.1.4 Image artefacts	54
3.2 Fabrication of abdominal Spectral CT phantom.....	54
3.2.1 Body phantom	56
3.2.2 Small cylindrical	57
3.2.3 Metal insertion compartment	58
3.3 Phantom positioning	59
3.3.1 Homogenous phantom scanning	60
3.3.2 Inhomogeneous phantom scanning	61
3.4 CT imaging parameters.....	62
3.5 Preparation of contrast media concentration	63
3.5.1 Barium.....	64
3.5.2 Iodine.....	65
3.5.3 Gadolinium.....	66
3.6 Development of metal artefact reduction algorithm	67
3.6.1 Image segmentation	69
3.6.2 Interpolation	70
3.6.3 Image filtering.....	71

3.7 Image analysis.....	74
3.7.1 Quantitative image analysis	74
3.7.1(a) Signal-to-noise ratio measurements.....	74
3.7.1(b) CT Image profile	75
3.7.2 Qualitative Image Analysis.....	75
CHAPTER 4 : RESULTS AND DISCUSSION	76
4.1 Quality assurance test of CT scanner.....	76
4.1.1 CT number accuracy	78
4.1.2 Image noise	79
4.1.3 Image uniformity.....	80
4.1.4 Image artefacts	81
4.2 Artefact severity for orthopaedic metal screw	82
4.3 CT Image Noise	84
4.3.1 Slice Thickness.....	85
4.3.2 Single-energy and dual-energy CT	87
4.4 Contrast media	89
4.4.1 Concentration 1	91
4.4.2 Concentration 2	93
4.5 Metal artefact reduction algorithm	98
4.6 Contrast media and metal artefact reduction algorithm.....	100
4.7 Limitations	110

CHAPTER 5 : CONCLUSION AND FUTURE WORK 111

5.1 Conclusion 111

5.2 Future work..... 113

REFERENCES 114

APPENDICES

ACADEMIC CONTRIBUTIONS

LIST OF TABLES

	Page
Table 3.1 The comparison of tolerance values for quality assurance test of CT machine between IAEA protocol and QAP (Malaysian protocol).....	52
Table 3.2 Summary of CT data parameters.....	62
Table 3.3 The concentration of contrast media used in this study for Concentration 1 and Concentration 2.....	64
Table 4.1 The tolerance values for quality assurance test of CT machine.....	77
Table 4.2 The <i>p</i> -value of contrast media; Iodine, Barium and Gadolinium of Concentration 1 and water-based phantom (stainless steel).....	93
Table 4.3 The <i>p</i> -value of contrast media; Iodine, Barium and Gadolinium of Concentration 2 and water-based phantom.....	94
Table 4.4 The <i>p</i> -value of contrast media; Iodine, Barium and Gadolinium of Concentration 1 and Concentration 2.....	97
Table 4.5 Table of contrast media image obtained at Concentration 1 before and after metal artefact reduction algorithm.....	103
Table 4.6 Table of contrast media image obtained at Concentration 2 before and after metal artefact reduction algorithm.....	104

LIST OF FIGURES

	Page
Figure 2.1	The electromagnetic spectrum shows the relationship between wavelength, frequency and energy. X-rays and γ -rays are part of the high energy electromagnetic spectrum (Seibert, 2004).... 11
Figure 2.2	Two types of X-ray radiation generated; (a) bremsstrahlung and (b) characteristic radiation (Wittke, 2006)..... 13
Figure 2.3	(a) The photoelectric effect in which an incident photon transfers all of its energy to inner shell electron and the electron is ejected out. (b) The electron from an outer shell may move down to fill in the vacancy and produce characteristic X-ray photon (Heggie et al., 2001)..... 15
Figure 2.4	The Compton scattering, in which an incident photon interacts with an outer shell of electron. Only a part of the incident photon energy is transferred to the electron, the photon itself is deflected from its original path (Heggie et al., 2001)..... 16
Figure 2.5	X-ray energy spectra produced in the dual-energy scanner at two different tube voltages of 80 and 140 kV. Retrieved from (Johnson et al., 2007)..... 19
Figure 2.6	Evolution of four generations of CT scanner. First and second CT scanner generation the beam and detector are translated and rotated across the area of interest. While for the third and fourth generation scanner, the fan beam is rotated to increase the scanning speed (Robb, 1982a)..... 21
Figure 2.7	The phase of CT image formation; the scanning data phase, reconstruction phase and digital-to-analogue conversion phase (Sprawls, 1988)..... 23
Figure 2.8	Diagram of CT scanning process which the patient is scanned with the X-ray source and detector rotates around the patient. Thin slice X-ray beams interact with the tissue and detector collect enough information from the interaction for image reconstruction (Illingworth, 2011)..... 24
Figure 2.9	(a) The original image of Sheep-Logan head phantom and (b) the corresponding sine wave sinogram (Cui et al., 2014)..... 25
Figure 2.10	CT image composed of a matrix of pixels, with each pixel representing a volume of tissue (voxel) (Wright and Grey, 2016)..... 27

Figure 2.11	CT image formation and reconstruction phase. (A) Data for a single-plane image is acquired. (B) Data of several plane images from multiple projections of 360o rotation around the patient is constructed. (C) Each plane of the image consists of a matrix of many voxels. (D) Combination of cuboid voxels allowed the formation of 3D images (E) (PocketDentistry, 2015).....	27
Figure 2.12	The CT Hounsfield scale for different kinds of human tissue (Kachelrieß, 2008).....	28
Figure 3.1	Overview of the methodology process conducted in this study.....	50
Figure 3.2	Placement of ROIs at central and peripheral on CT image with a diameter of 2 to 3 cm was drawn. Central ROI used for CT number accuracy and image noise; peripheral and central ROI for image uniformity (International Atomic Energy Agency, 2012).....	54
Figure 3.3	An abdominal Spectral CT phantom fabricated using PMMA materials.....	55
Figure 3.4	Schematic drawing of the phantom consisted of body part, small cylindrical and metal insertion part.....	55
Figure 3.5	The spectral CT body phantom of 32 cm diameter using PMMA materials, and consists of a small cylindrical tube and two water valves.....	56
Figure 3.6	A view of circular Spectral CT body phantom from (a) top, (b) side and (c) bottom.....	56
Figure 3.7	The small cylindrical of the diameter of 6 cm and was screwed individually in the abdominal body phantom.....	57
Figure 3.8	The dimension and view of the small cylindrical part from the (a) top and (b) side of the phantom.....	57
Figure 3.9	The metal insertion compartment consists of cylindrical body and a screwed cap with a diameter of 18 mm.....	58
Figure 3.10	The dimension and view of metal insertion compartment part of (a) cylindrical body and (b) a screwed cap.....	58
Figure 3.11	Schematic diagram of phantom positioning for CT imaging procedure. Phantom placed horizontally on the couch (U.S. Department of Health and Human Services., 2010). The diagram has been modified here to suit the thesis context.....	59

Figure 3.12	Schematic image of metal screw placement (yellow rectangular) in the phantom for homogenous phantom scanning. The abdomen and small tube cylinders phantom was filled with water.....	60
Figure 3.13	Schematic image of metal screw placement (yellow rectangular) in the phantom for inhomogeneous phantom scanning. The red small tube cylinder was filled with contrast media. The abdomen phantom was filled with water.....	61
Figure 3.14	The clinical contrast media used in this study; (a) Iomeprol 350 mgI/ml (Iomeron®), (b) 49 mg Ba/ml of Barium sulfate suspension (E-Z-Cat®) and (c) 0.5 mol formulation of Gadobenate dimeglumine (MultiHance®).....	63
Figure 3.15	Proposed steps for metal artefacts reduction algorithm.....	67
Figure 3.16	Histogram plot of CT images. The pixel value lies within the certain range (red region) that belongs to the certain class.....	69
Figure 3.17	Selection of intensity value (HU) for metal implant using histogram plot. The image segmentation of metal implant for high-energy image based on histogram plot was at 523 HU.....	69
Figure 3.18	Image pixel at an unknown point of A, and known point of B, C, D and E. An average of the pixel value at point B, C, D and E was interpolated at an unknown value at point A.....	71
Figure 3.19	The imaging principle for median filtering of 3 by 3 pixel. Input image was reconstructed by reordering the pixel values from the window into ascending order. Output image was produced by simply replaced the middle value from the sorted list.....	72
Figure 3.20	Comparison of a median filter, (a) Original Image, and the output image of (b) 3x3 median filter, (c) 5x5 median filter, (d) 7x7 median filter, (e) 8x8 median filter and (f) 9x9 median filter.....	73
Figure 3.21	The five circular area of 50 mm ² ROIs region was drawn surrounding of small PMMA tubes for the image analysis of metal artefacts severity.....	74
Figure 3.22	Line profile performed for CT image before and after applying metal artefacts reduction technique and contrast media.....	75

Figure 4.1	Placement of ROIs at central and peripheral on CT image of (a) body and (b) head water phantom with a diameter of 2 to 3 cm was drawn. Central ROI used for CT number accuracy and image noise; peripheral and central ROI for image uniformity.....	77
Figure 4.2	The CT number of water for body and head phantom. The orange line represents the tolerance limit of the CT number of water, which is ± 5 HU of the baseline value.....	78
Figure 4.3	The CT number of air for body and head. The purple line represents the tolerance limit of the CT number of air as stated by IAEA (International Atomic Energy Agency, 2012).....	79
Figure 4.4	The standard deviation of water for body and head phantom. The blue straight line represents the tolerance limit of the standard deviation of water as stated by IAEA (International Atomic Energy Agency, 2012).....	80
Figure 4.5	The absolute difference of CT number between central and peripheral ROI for body and head phantom. The red straight line represents the tolerance limit as stated by IAEA (International Atomic Energy Agency, 2012).....	81
Figure 4.6	CT image of artefact evaluation at window level of 0, and window width of (a) 50 (b) 100 and (c) 500.....	81
Figure 4.7	CT images of metallic artefacts severity from (a) stainless steel ($Z=26.7$) and (b) titanium alloy ($Z=21.4$)	82
Figure 4.8	The signal-to-noise ratio against slice thickness for titanium alloy and stainless steel in CT imaging. The signal-to-noise ratio is approximately linear for titanium alloy and stainless steel ($R^2 = 0.9812$ and $R^2 = 0.9632$ respectively) with slice thickness.....	83
Figure 4.9	The CT slices of the water-based phantom obtained at different slice thickness: (a) 1 mm, (b) 3 mm and (c) 5 mm. The CT image noise depends on the number of X-ray photons contributing to the image.....	85
Figure 4.10	The signal-to-noise ratio against slice thickness from scans of a water-based phantom. The signal-to-noise ratio is approximately linear ($R^2 = 0.9632$) with slice thickness.....	86
Figure 4.11	The signal-to-noise ratio against slice thickness for single-energy and dual-energy CT from scans of a water-based phantom. The signal-to-noise ratio is approximately linear for dual-energy and single-energy CT ($R^2 = 0.9632$ and $R^2 = 0.9711$ respectively) with slice thickness.....	88

Figure 4.12	The CT image of stainless steel for differences contrast media; Iodine, Barium and Gadolinium obtained at (a) Concentration 1 and (b) Concentration 2.....	90
Figure 4.13	The signal-to-noise ratio against slice thickness of water-based phantom with contrast media (Concentration 1) before metal artefact reduction algorithm.....	91
Figure 4.14	The signal-to-noise ratio against slice thickness of water-based phantom with contrast media (Concentration 2) before metal artefact reduction algorithm.....	93
Figure 4.15	The signal-to-noise ratio of Iodine at Concentration 1 and Concentration 2 as a function of slice thickness.....	95
Figure 4.16	The signal-to-noise ratio of Barium at Concentration 1 and Concentration 2 as a function of slice thickness.....	96
Figure 4.17	The signal-to-noise ratio of Gadolinium at Concentration 1 and Concentration 2 as a function of slice thickness.....	97
Figure 4.18	The CT image of water phantom (stainless steel) (a) before and (b) after applying metal artefact reduction algorithm and (c) CT number profile through the beam hardening artefacts of the image.....	98
Figure 4.19	The CT image of water phantom (titanium alloy) (a) before and (b) after applying metal artefact reduction algorithm and (c) CT number profile through the beam hardening artefacts of the image.....	99
Figure 4.20	The CT images of Iodine contrast (Concentration 1) (a) before and (b) after applying metal artefact reduction algorithm. (c) The CT number profile through the beam hardening artefacts of the phantom.....	101
Figure 4.21	The signal-to-noise ratio against slice thickness of contrast media (Concentration 1) after beam hardening reduction and filtering algorithm.....	105
Figure 4.22	The CT images of Iodine contrast (Concentration 2) (a) before and (b) after applying metal artefact reduction algorithm technique. (c) The CT number profile through the beam hardening artefacts reduction and filtered image of the phantom.....	106
Figure 4.23	The signal-to-noise ratio against slice thickness of water-based phantom with contrast media (Concentration 2) after metal artefact reduction algorithm.....	107

Figure 4.24	The comparison of signal-to-noise ratio before and after applying metal artefact reduction algorithm for Iodine at Concentration 1.....	108
Figure 4.25	The comparison of signal-to-noise ratio before and after applying metal artefact reduction algorithm for Iodine at Concentration 2.....	108
Figure 4.26	The comparison of signal-to-noise ratio before and after applying metal artefact reduction algorithm for Gadolinium at Concentration 1.....	108
Figure 4.27	The comparison of signal-to-noise ratio before and after applying metal artefact reduction algorithm for Gadolinium at Concentration 2.....	109
Figure 4.28	The comparison of signal-to-noise ratio before and after applying metal artefact reduction algorithm for Barium at Concentration 1.....	109
Figure 4.29	The comparison of signal-to-noise ratio before and after applying metal artefact reduction algorithm for Barium at Concentration 2.....	109
Figure 5.1	The signal to noise ratio against slice thickness of water-based phantom with contrast media (Concentration 1) before metal artefact reduction algorithm.....	129
Figure 5.2	The signal to noise ratio against slice thickness of water-based phantom with contrast media (Concentration 2) before metal artefact reduction algorithm.....	129
Figure 5.3	The signal to noise ratio against slice thickness of water-based phantom with contrast media (Concentration 1) after metal artefact reduction algorithm.....	130
Figure 5.4	The signal to noise ratio against slice thickness of water-based phantom with contrast media (Concentration 2) after metal artefact reduction algorithm.....	130

LIST OF ABBREVIATIONS

1D	One-dimensional
2D	Two-dimensional
3D	Three-dimensional
AEC	Automatic exposure control
ALARA	As low as reasonably achievable
CT	Computed Tomography
DICOM	Digital Imaging and Communications in Medicine
FBP	Filtered back projection
FOV	Field of view
HU	Hounsfield unit
IAEA	International Atomic Energy Agency
ICRU	International Commission on Radiation Units
kV	kilovoltage
MARs	Metal artefacts reduction software
MATLAB	Matrix Laboratory
MDT	Metal deletion technique
MTF	Modulation transfer function
PMMA	Polymethyl methacrylate
PVE	Partial volume effect
ROI	Region of interest
SNR	Signal-to-noise ratio

**PEMBANGUNAN TEKNIK PASCA-PEMROSESAN BAGI
PENGURANGAN ARTIFAK LOGAM DENGAN KEHADIRAN KONTRAS
MEDIA DALAM PENGIMEJAN CT**

ABSTRAK

Artefak yang timbul daripada logam implan dalam pengimejan CT telah menjadi kebimbangan untuk mendapatkan kualiti imej yang optimum. Matlamat penyelidikan ini adalah untuk membangunkan teknik pasca pemrosesan dan menggunakan kehadiran kontras media bagi mengurangkan keterukan artifak logam daripada skru ortopedik dalam pengimejan CT abdomen. Pengenalpastian imej CT samada dalam atau berhampiran implan metalik perlu diramalkan semasa pengimejan, bagi menilai penyakit dan membolehkan analisis imej yang lebih baik terhadap pesakit untuk pengesanan awal penyakit dan pencegahan peristiwa penyakit akut. Kajian ini dilakukan dengan menggunakan fantom abdomen berasaskan air yang besaiz diameter 32 cm (saiz badan dewasa). Fantom dibuat menggunakan bahan PMMA. Skru logam ortopedik (keluli tahan karat gred 316L dan titanium aloi gred 5) diletakkan di dalam setiap tiub PMMA kecil secara berasingan. Sebanyak 100 ml kontras media (Iodin, Barium dan Gadolinium) dengan Kepekatan 1 dan Kepekatan 2 dengan masing-masing diisi dalam tiub PMMA kecil dan diletakkan di dalam badan fantom. Phantom yang direka itu diimbas dengan tenaga tunggal CT (120 kV) dan dwi-tenaga CT (80/140 kV). Mod imbasan telah ditetapkan menggunakan tetapan kawalan dedahan automatik dan imbasan telah ditetapkan pada pic 0.60 dan ketebalan kepingan 1.0, 3.0, dan 5.0 mm. Imej CT yang diperolehi kemudiannya diproses dengan algoritma pengurangan artefak logam yang dicadangkan. Gambar-gambar sebelum dan selepas penggunaan algoritma pengurangan artifak

kemudiannya dikira nisbah isyarat-ke-hingar. Dalam kajian ini, penggunaan kontras media mampu meningkatkan ketepatan sempadan organ, menunjukkan perbezaan antara tisu-tisu, dan meningkatkan keterlihatan tisu badan. Di samping itu, algoritma pengurangan artifak logam yang dibangunkan dapat mengurangkan artefak dan bunyi gambar, dan dengan itu dapat meningkatkan kualiti imej CT diperolehi. Gabungan kedua-dua teknik ini dapat meningkatkan nisbah isyarat-ke-hingar, mengurangkan artefak dan gambar hingar, justeru dapat menyediakan maklumat pengimbasan imej yang cukup berhampiran implan logam. Skru logam dalam pengimejan CT dapat dioptimumkan pada $\text{pic} = 0.60$, dan ketebalan kepingan = 5.0 mm. Oleh itu, gabungan optimum parameter dalam protokol CT, aplikasi kontras media dan algoritma pengurangan dapat menghasilkan maklumat imej yang lebih tepat dan kualiti imej yang lebih baik dalam bidang implan metalik.

**DEVELOPMENT OF POST-PROCESSING TECHNIQUE FOR METAL
ARTEFACTS REDUCTION IN THE PRESENCE OF CONTRAST MEDIA IN
CT IMAGING**

ABSTRACT

Artefacts arising from metallic implant in CT imaging had been a concern in obtaining an optimal image quality. The objective of this research is to develop the post-processing technique to reduce the severity of metal artefacts from orthopaedic screw in the presence of contrast media in abdominal CT imaging. Identification of CT images within or near metallic implants should be predicted by imaging, the assessment of disease would be refined, allowing better image analysis of patient for early detection and prevention of acute disease events. This study is performed by using a water-based abdomen phantom of diameter 32 cm (adult body size). The phantom is fabricated using PMMA material. The orthopaedic metal screw (stainless steel grade 316L and titanium alloy grade 5) is placed in each small PMMA tube separately. A 100 ml of contrast media (Iodine, Barium and Gadolinium) of Concentration 1 and Concentration 2, is filled in a small PMMA tube and placed inside a body phantom respectively. The fabricated phantom is scanned with single-energy CT (120 kV) and dual-energy CT (80/140 kV). The scan modes are set using Automatic Exposure Control setting and the scans are set at pitch of 0.60 and slice thickness of 1.0, 3.0, and 5.0 mm. The CT image obtained is then post-processed with the metal artefact reduction algorithm proposed. The images before and after applied metal artefact reduction algorithm is then calculated the signal-to-noise ratio. In this phantom study, the usage of contrast media able to improve the accuracy of border delineating organ of interest, exhibit contrast between tissues of interest, and

improve visibility of body tissue. Moreover, the proposed metal artefact reduction algorithm is developed to reduce the beam hardening artefact and image noise, and thus improve CT image quality obtained. The combination of these two techniques increased the signal-to-noise ratio, reduced beam hardening artefact, image noise, and hence providing enough image scanning information near metallic implant. The imaging CT of metal screw is optimised at pitch = 0.60, and slice thickness = 5.0 mm. Therefore, combination of optimised parameters of CT protocol, contrast media application and reduction algorithm results in an improved image information and image quality in the area of metallic implants.

CHAPTER 1

Introduction to the Thesis

The metal artefact reduction technique is being developed for the use in clinical healthcare. The long term objective of this research is to improve the clinical diagnosis of the implant itself, the interface between the implant and the bone and surrounding tissues by the application of Computed Tomography (CT). The first section of this Chapter describes the thesis objective. The following sections focus on the clinical and technical background of this research. This is followed by the sections of the motivation and the clinical significance of this study. Finally, the thesis organization is provided, followed by a summary of this Chapter.

1.1 Objectives

1.1.1 The thesis objective

The main objective of this research is to develop the post-processing technique to reduce the severity of metal artefacts from the orthopaedic screw in the presence of contrast media in abdominal CT imaging.

The specific objectives involved in the process of achieving the thesis objective are as follows:

1. To determine the artefact severity in single-energy CT and dual-energy CT scan mode for titanium alloy and stainless steel in abdominal imaging.
2. To develop the metal artefact reduction algorithm in CT imaging.

3. To evaluate the image artefact severity after applying metal artefact reduction algorithm in the presence of contrast media.
4. To compare the image of metal artefact reduction before and after applying the developed metal artefact reduction algorithm and contrast media.

1.2 Clinical and technical background

CT is widely used as imaging modality in the management of chest, abdomen and pelvis for diagnosis, treatment planning and clinical studies because it provides detailed image views of all types of human body tissues (Sharma and Aggarwal, 2010). However, a limitation with CT imaging would be the difficulty to evaluate image with the artefacts arising from metallic implants in patient's body (Lee et al., 2007). Metal implants such as dental fillings, joint prostheses, implanted marker bins, coils, wires, pedicle screw placement, stenting, and clipping, usually undergo follow-up CT imaging (Campi et al., 2007; Yu et al., 2009a; Schulze et al., 2011).

The numbers of patient receiving metal implants showed a significant increase since the advanced of orthopaedic surgery. For example in the United States, the number of hip replacements among patients aged 45 is doubled from 2000 to 2010 (Wolford, et al., 2015). Apart that, the number of patients diagnosed with prostate cancer along with hip prosthesis is also increased (Giantsoudi et al., 2017). In such cases as prostate cancer with hip implants, the metal artefact may present within or close to the area may greatly affect the diagnosis and treatment process for patients. The process is difficult with the artefacts presented due to the extreme photon absorption by the metal object.

In the presence of metal implant, it is essential to assess the implant itself, the interface between the implant and the bone and the surrounding tissues of the implant. These diagnostic criteria are important to prevent cracking or loosening and sufficient verification with adequate protection of the implant (White and Buckwalter, 2002) and ruling out of hematoma or inflammation in the adjacent soft tissue. However, due to the occurrence of metal artefacts, the diagnosis on CT images remains challenging with many cases rendered uninterpretable, even with hard convolution kernels and widened CT density ranges (Lee et al., 2007). For treatment planning of radiation therapy, the implants existed within or close to the treatment cause the difficulties in either to delineate the target volume or organ at risk or by reducing the dose calculation accuracy (Pettersson, 2015).

This is because these metallic implant leads to severe streak and shadow artefacts in CT images that superimpose the structures of interest and deteriorate image quality, which is important for diagnostic imaging (Yu et al., 2009a; Zhang et al., 2011). Metal objects have a very high density, which is strongly attenuated to the transmitted X-ray beam during CT examination. It results in the production of severe image artefacts in the form of streak and shadow artefacts, due to the lack of data in the projection data in CT images (Manzke et al., 2004).

A numbers of simple methods employed to reduce the amount of metal artefacts by altering the technical parameters of the CT protocol. For example, increasing tube kilovoltage, increasing tube current, decreasing the pitch (Link et al., 2000; Vande et al., 2006), and increasing the slice reconstruction thickness (Stradiotti et al., 2009). However, these techniques do not remove artefacts completely.

Other than altering the CT protocol parameters, metal artefact reduction algorithm also has been developed to reduce metal artefacts. The most commonly used is filtered back projection (FBP), interpolation and iterative reconstruction methods. These methods involved in the replacement of the metal-corrupted data due to metallic implants. These methods have been shown to reduce the degree of metal artefacts; however these techniques are not widely available. Moreover, these methods also do not remove all sources of streaking artefacts, cause loss of spatial resolution in images and introduce the secondary artefacts that may lead to misinterpretation (Bamberg et al., 2011; Boas and Fleischmann, 2011; Lee et al., 2012).

The other studies used iterative reconstruction algorithm technique to replace the corrupted data of metal artefacts on CT images and thus reduce streaking artefacts due to beam hardening, photon starvation, and edge effects (Hara et al., 2009; Prell et al., 2009). However, the limitations of this technique is the implementation involved high computational cost which requires specialized processor units and the needs of the combination of sinogram image with iterative reconstruction algorithm which cause the metal artefacts is rather severe in CT images (Lemmens et al., 2009; Chen et al., 2009).

In addition, Lambert et al. introduced another technique to reduce metal artefacts severity is by using contrast media which has higher K-edge than the metal implant. They introduced new contrast media; tantalum, tungsten, bismuth, and is unrealistic for clinical use. This is due to the factor neglected in this study such as concentration, toxicity, and circulation time of the contrast media (Lambert et al., 2015).

The advantages of contrast media are able to increase the detection of soft tissue and blood vessel surrounding the metal implant. This is because the materials with K-edges at higher X-ray energy are attractive in CT imaging; their attenuation is greater at the higher keV levels, therefore their K-edges are near effective X-ray spectrum's mean energy. Contrast enhancement begins to diminish for materials with K-edge energy levels above the effective X-ray spectrum's mean energy (Lambert et al., 2015).

The use of novel (non-iodinated) contrast media such as bismuth, tantalum and tungsten had been studied as potential CT imaging contrast agents. However, the application of novel contrast media is particularly challenging as it would require the biological safety evaluation first before being approved for the clinical practice. This is relatively due to the present of foreign materials that needs to be injected into the vascular system of the patients.

Meanwhile, the use of conventional contrast media such as iodine, barium and gadolinium which is already approved for clinical use is safer compared to the novel contrast media. The foreign materials present in contrast media is already studied and proved to be safe to be injected into patient's body.

1.3 Motivation of the study

This study is motivated by the presence of the metal artefacts from metallic implants in spectral CT imaging, which lead to severe streak and shadow artefacts in CT images that superimpose the structures of interest and deteriorate image quality, which is important for diagnostic imaging. It is essential to assess the implant itself, the interface between the implant and the bone and also the surrounding tissues nearby implant. These diagnostic criteria is important to prevent cracking or

loosening and implant verification with adequate protection of the implant (White and Buckwalter, 2002) and prevent inflammation in the adjacent soft tissue.

Apart from evaluating the metal implants, a CT scan is also needed for patients who may have a metal implant to diagnose problems such as tumour, cancer, cardiovascular disease and so on. This is due to the need for proper size and dimensions of a disease for diagnosis and treatment planning procedures is indispensable. Although there is a need for an accurate assessment of CT images with a metal implant, the diagnosis on CT images remained challenging with many cases rendered uninterpretable. Moreover, this metal implant also contributed scattered radiation towards organ nearby the metal implant which may harm the sensitive organ.

The application of various developed of metal artefact reduction techniques for metallic implants in CT images do not achieve widespread clinically used. This is mainly because they do not remove all sources of streaking, cause loss of spatial resolution in images, and they also introduce the secondary artefacts. Other than that, CT imaging without contrast enhancement contribute to a limited diagnostic use including detection of active bleeding, vascular stenosis, or the presence of infection or soft tissue injury, which frequently occur near the metallic implant.

Therefore, the combinations of image metal artefact reduction algorithm and contrast media techniques are able to diminish the streaking artefacts due to the metal implant and enable to extract information about the organ of interest. Besides providing the usefulness of these techniques in diagnostic imaging; this is also providing very important information for the treatment planning procedure to detect the exact and enough information about the region of interest (ROI).

1.4 Clinical significance

This ability of the metal artefact reduction in CT imaging using metal artefact reduction technique with the presence of clinical contrast media to obtain high quality image together with the high resolution images and allows more spectral information. The combinations of these two techniques are able to reduce the reconstruction errors by supplementing correct information in the projection images and also by integrating the incorrect information to form useful information of images. This research performed is able to suppress most artefacts produced by metal implants, represents a contribution to the diagnostic imaging of metallic implants. With continuing developments of the metal artefact reduction algorithm, it should be possible to translate this technique together with contrast media technique onto a clinical imaging that allows a better visualization prior to the diagnosis. These findings would be a highly significant advance in clinical imaging. If the vicinity of the artefacts from metallic implants could be diagnosed by imaging, this allowing an ability to diagnose and interprets disease accurately due to the reduction of the artefacts. This would markedly improve the diagnosis of the diagnosing the implant itself, the interface between the implant and the bone and also the surrounding tissues nearby the implants.

1.5 Thesis organisation

This thesis consists of five Chapters and is structured as follows:

This thesis begins with Chapter 1, the introduction Chapter. This Chapter includes five sub topics. The subtopics cover on objectives of the study, clinical and technical background, the motivation of the study, clinical significance, thesis organization and summary of the Chapter.

Chapter 2 focuses on the theory and literature review. It discusses the historical and basic principle of X-ray and conventional CT imaging. This Chapter explains about X-rays, how they are produced, and also how they interact with matter. It also describes the evolution of CT technology and the basic principles of CT imaging. Characteristics of CT image are also discussed in this Chapter which includes contrast, spatial resolution, noise and artefacts are also described. This Chapter also explains in the literature review of the previous study that is related to this work including imaging parameters, metal artefact reduction techniques and contrast media techniques.

Chapter 3 presents the materials and methodology of this project. It explains the quality control tests performed on CT machine, which include CT number accuracy, image noise, image uniformity and image artefacts test. This Chapter also presents the phantom design and fabrication phantom positioning during the scanning and CT parameters used for the scanning. Next, the preparation of the contrast media concentrations is covered as well as the steps for development of metal artefact reduction algorithm. The image analysis of the signal-to-noise ratio and statistical analysis are also presented.

Chapter 4 describes the quality assurance tests of CT scanner; including CT number accuracy, image noise, image uniformity and image artefacts as well as the data acquired on CT image noise for the image at different slice thickness and dual-energy and single-energy CT. Artefact severity for different orthopaedic implants is also discussed. The applications of the introduced method; including contrast media, metal artefact reduction, and the combination of both techniques are also included. This is followed by the discussion and explanation of each result obtained.

Chapter 5 describes the conclusions and recommendations for the future works.

Finally, the list of references and appendices are attached.

CHAPTER 2

Theory and literature review

This Chapter focuses on the theory and literature review. It discusses the historical and basic principle of X-ray and conventional CT imaging. It explains about X-rays, how they are produced, and also how they interact with matter. It also describes the evolution of CT technology and the basic principles of CT imaging. Characteristic of CT images are also discussed in this Chapter which includes contrast, spatial resolution, noise and artefacts. Literature review about the previous study on CT, imaging parameters, metal artefact reduction techniques and contrast media is also presented in this Chapter.

2.1 X-rays

X-rays are discovered by Wilhelm Conrad Rontgen in 1895 and he has received numerous honours for his discovery of X-rays, including the first Nobel Prize in 1901 (Grieken and Markowicz, 2001). He discovered X-ray by detecting electromagnetic radiation that contains both electrical and magnetic fields. Electromagnetic radiation is also described as a stream of photons, with each of them has energy and travels at a velocity of light.

A relationship between the velocity of light (c), frequency (f) and wavelength (λ) is described in Equation 2.1. The velocity of the electromagnetic radiation travels in a vacuum is $c = 3.0 \times 10^8 \text{ ms}^{-1}$. The length of time that light travels in 1 cycle is the period and is described in units of seconds (s), and frequency is the number of cycles per seconds (s^{-1}) or Hertz (Hz). Wavelength is a distance travelled by

electromagnetic radiation in a cycle, usually described in units of nanometers (10^{-9} m).

$$c = \lambda f \quad (2.1)$$

Each photon of electromagnetic radiation contains a certain amount of energy. The electromagnetic spectrum shows the amount of energy contains in electromagnetic radiation, which ranges from low energy radiation to a high energy radiation as shown in Figure 2.1. The relationship between photon energy and frequency of electromagnetic radiation is described as shown in Equation 2.2.

$$E = hf \quad (2.2)$$

The photon energy (E) is directly proportional to the frequency of the wave (f), where h is a Planck's constant, $h = 6.62 \times 10^{-34} \text{ Js}^{-1} = 4.13 \times 10^{-21} \text{ eVs}^{-1}$. The higher the frequency of the electromagnetic waves, the higher the photon energy (Seibert, 2004).

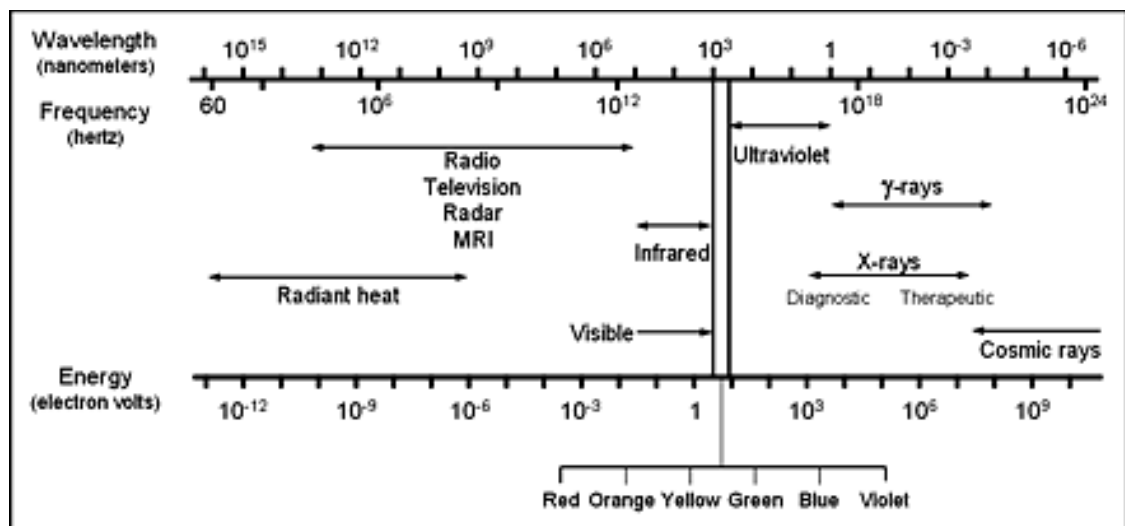


Figure 2.1. The electromagnetic spectrum shows the relationship between wavelength, frequency and energy. X-rays and γ -rays are part of the high energy electromagnetic spectrum (Seibert, 2004).

2.1.1 Generation of X-rays

The process of X-ray generation in an X-ray tube is very inefficient because mostly about 99% of the electron beam from the accelerated electron is being converted to heat, while the remaining 1% is converted to X-ray. The process of generating X-ray beam for research purposes, medical diagnostics imaging and so on, is started by accelerating the electrons in the evacuated environment of the X-ray tube with high velocity to the target metal. When the voltage is applied to the circuit results in a large increase in tube current, it causes intense heating of the filament due to its electrical resistance. The highly energetic electrons are released by a process of thermionic emission due to the potential difference between the cathode and anode. A high speed of electrons is accelerated from the filaments of cathode towards a positive target anode. The rotating anodes will dissipate the heat generated and X-rays are generated within the target anode and an X-ray beam is directed towards the patient.

When the electrons hit the target anode, two types of X-ray radiation are generated; *bremstrahlung* and characteristic radiation. *Bremstrahlung* or braking radiation is generated when the high velocity of electrons suddenly slowed down as they are attracted to the positively charged nucleus, and their path is deflected. As the electrons slow down, they give off energy in the form of *bremstrahlung* or braking radiation. Meanwhile, the characteristic X-ray is generated when a high energy electron collides with an inner shell electron. If the bombarding electrons have sufficient energy, they can eject out an electron out of the inner shell of the target metal atoms leaving a 'hole' in the inner layer. Then, the electron from the higher states drop down to fill the vacancy with a loss of energy emitted as an X-ray photon (Seibert, 2004).

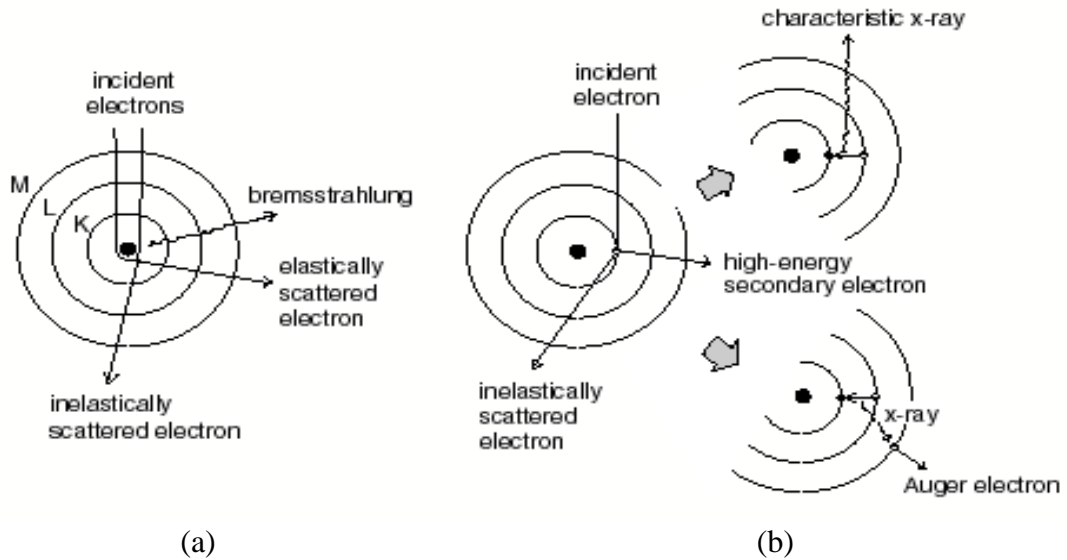


Figure 2.2. Two types of X-ray radiation generated; (a) *bremsstrahlung* and (b) characteristic radiation (Wittke, 2006).

2.1.2 Interaction of X-ray with matter

X-ray imaging relies on the differential attenuation of photon beam when passing through an object being imaged. As the beam interacts with matter, it produces a variable transmitted X-rays either the X-rays radiation will be absorbed, scattered or penetrated without interacting with anatomical structures. The denser the tissues, the more X-rays are attenuated. For example, bone attenuates more X-rays radiation compared to lung tissue. There are several interactions that can occur when X-rays radiation interacts with matter at diagnostic energy level, including, photoelectric absorption, Compton scattering, and Rayleigh (coherent) scattering.

Photoelectric absorption is the process of photon beam interacts with an electron in an inner shell that has a binding energy similar to or less than the energy of incident X-ray beam as shown in Figure 2.2. Photoelectric absorption can take place if the energy of the incident photon has slightly more energy than the binding energy of the inner electron, and attenuation occurs. However, photoelectric absorption cannot

occur if the incident photon energy is less than the binding energy of the electron. The incident energy of photon which has slightly more energy than the inner electron will transfer its energy to the inner electron and overcome the binding energy of the inner orbital electron and the electron is ejected from its shell. The remaining energy left is given to the ejected electron and then is deposited near the site of interaction. The kinetic energy of the ejected electron is equal to the difference of the incident photon energy, E_0 and the binding energy of the inner shell electron, E_{EE} as defined in Equation 2.3.

$$KE = E_0 - E_{EE} \quad (2.3)$$

This interaction will create the vacancy in the inner orbital shell, named as K shell and this vacancy must be filled with another electron from an outer shell, named as L shell to create the atom stability. The electron with lower binding energy from an outer shell moves down to fill in. The drop in energy to fill the vacancy will produce characteristic X-ray photon, in which the energy is equal to the difference in electron binding energy of the inner shell electron and outer shell electron. The probability of photoelectric absorption is related to the atomic number of the material (Z) and the energy of the incident photon (E), in which is approximately proportional to Z^3/E^3 . The photoelectric absorption is increasing with increasing atomic number of the absorber atom and decreasing incident photon energy. These facts explain the attenuation differences between low- Z materials (water and soft tissue) and high- Z materials (lead and bone). Therefore, the photoelectric interaction is important for signal contrast in X-ray imaging.

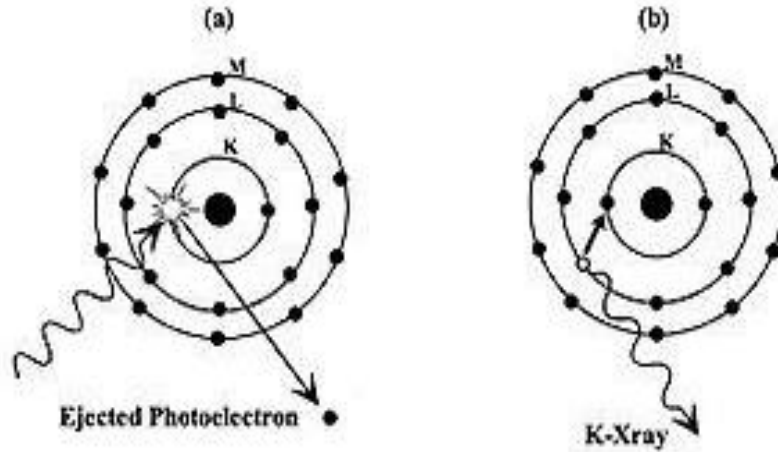


Figure 2.3. (a) The photoelectric effect in which an incident photon transfers all of its energy to inner shell electron and the electron is ejected out. (b) The electron from an outer shell may move down to fill in the vacancy and produce characteristic X-ray photon (Heggie et al., 2001).

Compton scattering is the interaction between the outer shell of electron and incident X-ray photon, E_0 , which has much greater energy than the binding energy of an electron as shown in Figure 2.3. The incident photon interacts with electron which has a weak binding energy. The incident photon is ejected out the electron from its orbital position at an angle, ϕ and the electron gain energy. The incident photon with remaining energy, E_{IE} transferred is deflected from its original path with a trajectory at an angle, θ with respect to its original direction. The energy of the recoil electron, E_{RE} is defined as in Equation 2.4.

$$E_{RE} = E_0 - E_{IE} \quad (2.4)$$

The energy transferred of the recoil electron only depends on a photon-electron interaction. The scattered photon may travel in any direction from an angle of 0° to 180° from its original direction, while the recoil electron may only travel at an angle from 0° to 90° . The scattered photon may undergo another process of photoelectric absorption or Compton scattering in the anode or may escape the anode (Nikjoo et

al., 2012). Therefore, the Compton interaction is important for energy absorption of the soft tissues in X-ray imaging.

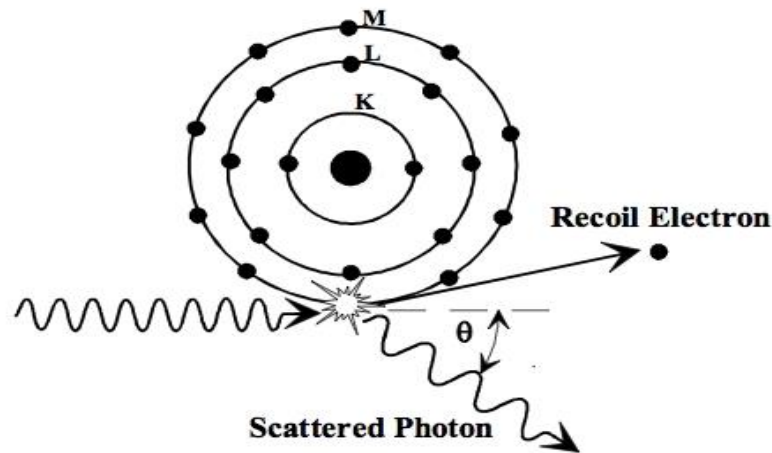


Figure 2.4. The Compton scattering, in which an incident photon interacts with an outer shell of electron. Only a part of the incident photon energy is transferred to the electron, the photon itself is deflected from its original path (Heggie et al., 2001).

Rayleigh scattering or also known as coherent scattering occurs when an incident photon interacts with inner shell electrons and is deflected or scattered with negligible loss of energy. There is no absorption of energy and the scattering of the incident photon is in the forward direction and most of the photon beams are scattered with a small angle from the original path. The probability of this event to occur is low and it is a minor contributor to the absorption coefficient.

2.1.3 The energy dependence of X-ray attenuation

The attenuation coefficient (μ) describes the energy reduction of the incident photon as it passes through matter, it experiences changes in its intensity; either by absorption or scattering events. This event occurring is dependent on the energy of the incident photon, thickness of a material, density of a material and the atomic number of a material. The total attenuation occurs depend on the types of interactions

occurs; photoelectric absorption, Rayleigh scattering and Compton scattering. The energy of the incident photon decreases exponentially with the distance travelled, as in Equation 2.5.

$$I = I_0 e^{-\mu x} \quad (2.5)$$

where, I is the X-ray beam intensity after travelling at a distance, I_0 is the initial X-ray beam intensity, μ is the attenuation coefficient, and x is the distance travelled.

The photoelectric effect is dominant at lower X-ray energies, in which approximately as E^{-3} . On the other hand, the attenuation of Compton scattering interactions is dominant at higher energies, approximately as E^{-1} at low Z materials. At high energies, the Compton scattering interaction is important for energy absorption of the soft tissues in diagnostic X-ray imaging. These explain that the photoelectric absorption and Compton scattering interaction aids the ability to detect the differences between low- Z materials, such as water and soft tissue and high- Z materials, such as lead and bone.

The probability of the Rayleigh scattering interaction to occur in soft tissue is low, which comprises about 10% of the interaction in mammography and 5% in chest imaging. While for the pair production interaction, extremely high energies are required for such interaction to occur. Therefore, CT imaging is largely dependent on the different X-ray attenuation with matters.

2.2 Computed Tomography

X-ray imaging has been used for over a century, after the discovery of X-rays in 1895 by Wilhelm Conrad Roentgen (Röntgen, 1896; Swinton, 1896). In diagnostic X-ray imaging, the two-dimensional (2D) transmission image is formed. Other than that, the projected image of the X-rays imaging causes an overlapping part of the soft tissue and bone structures can be difficult to interpret the exact size, shape and positions of objects. Furthermore, the projected image of X-rays imaging has very limited ability to differentiate between the low-contrast tissues.

Therefore, the introduction of CT in the early 1970s is a major step to overcome many of the problems in diagnostic imaging. CT imaging is used to overcome the limitation of X-rays imaging by producing an image of three-dimensional (3D) transmission. Other than that, CT imaging can be reconstructed the image of internal structures from multiple projections of the object. During the years since its introduction, CT has been dramatically improved in performance from the refinements in components to the innovation in scanning techniques. As a result, the scan speed, image resolution details and also the volume coverage of an object has been improved, in order to maintain patient comfort and safety (Ledley et al., 1974; Robb, 1982b). Hounsfield and Cormack demonstrated the mathematics behind tomographic images for real objects. They are then awarded the Nobel Prize in 1979 for their remarkable findings (Nobelprize, 1979).

The use of CT technology in imaging has been growing rapidly since the introduction of it. Recent advances in CT technology have been the introduction of two photon spectra that allow the uses of two different X-ray photon spectra. This is also known as spectral CT or dual-energy CT. This advanced technology of CT

continuously contributes to an increase in the clinical and diagnostic imaging value of CT. Two different energies are generated either by fast voltages switching of one X-ray tube or by running two X-ray tubes at different tube voltages. The attenuation information is gained from these two different X-ray spectra (80 and 140 kV). The difference between these two X-ray spectra is shown in Figure 2.4.

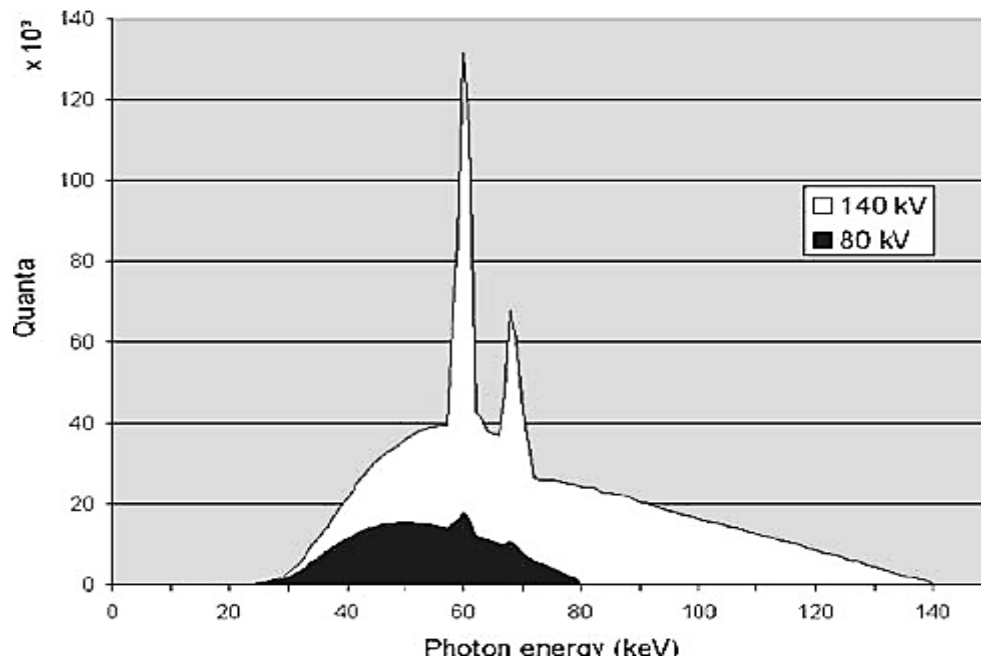


Figure 2.5. X-ray energy spectra produced in the dual-energy scanner at two different tube voltages of 80 and 140 kV. Retrieved from (Johnson et al., 2007).

The use of two different X-ray spectra can differentiate materials based on their X-ray attenuation (Avrin et al., 1978). Attenuation of the materials is caused by absorption and scattering of the X-ray photon. There are two main mechanisms that happened at low and high energy spectra; that are Compton scattering and photoelectric effect. This technique exploits attenuation difference especially for the materials with high atomic numbers due to the photoelectric effect (Kruger et al., 1977; Riederer and Mistretta, 1977). For example, attenuation of Iodine is much lower at high tube voltage settings than at low tube voltage settings. Therefore, the

enhancement of Iodine is brighter at low tube voltage setting (Nakayama et al., 2005; Kalva et al., 2006).

2.2.1 Evolution of CT scanner

CT scanner as first introduced in 1960's by Sir Godfrey Hounsfield. The first CT scanner generation is performed on the first brain-scan in 1971 (Hounsfield, 1980). Since the development of the first generation of CT scanners, it has undergone several technical advancement toward an improvement in scanning time and image quality.

There are four generations of CT scanners as in Figure 2.5. For the first and second CT scanner, the photon beam and detector are translated and rotated. The X-ray source and detector move horizontally across the field of view (FOV). The first generation of CT scanner use single pencil beam with a single detector and the beam is translated and rotated, which take long scanning times. In the second generation scanner, the pencil beam is replaced by a partial fan beam. The fan beam is again translated and rotated with multiple angles obtained with a single translation across the patient; which decrease the scanning time compared to the first generation.

For the third and fourth generation scanners, the fan beam is rotated to cover the entire FOV and increase the scanning speed. In the third generation, the beam is a fan-shaped beam and rotated along with the detector array, which is able to scan the entire angle area. For the fourth generation, only the X-ray source rotate around the patient while the detector array is fixed (Cunningham and Judy, 1999).

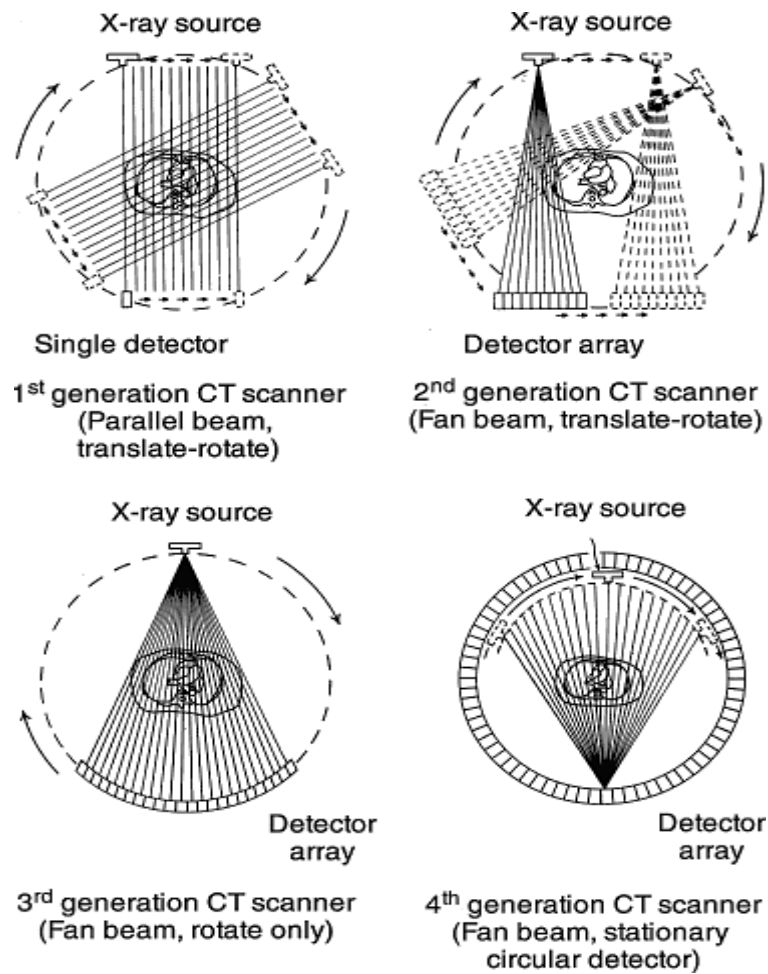


Figure 2.6. Evolution of four generations of CT scanner. First and second CT scanner generation the beam and detector are translated and rotated across the area of interest. While for the third and fourth generation scanner, the fan beam is rotated to increase the scanning speed (Robb, 1982a).

2.2.2 Basic principles of CT imaging

The basic components of CT scanner are the X-ray source, detector and object. Unlike a conventional X-ray which uses a fixed X-ray source, a CT scanner uses a motorized X-ray source that rotated around the gantry. The X-rays are generated in an X-ray tube by accelerating electrons with high voltage and allowing them to collide with target anode (tungsten), which has a high atomic number of materials in an X-ray tube. Rotating anode is used in the X-ray tube with the purpose to increase heat dissipation.

The energy of the accelerating electrons is the potential difference between anode and cathode. This is usually expressed as the kilovoltage (kV). X-rays are produced when the kinetic energy of the electrons is suddenly slowed down or stopped by a nucleus of the target anode. The lowest energy of photon beams is absorbed by the X-ray filters. This is due to the lowest energy of these X-rays photon does not contribute to the formation of the image but only will add to the patient dose. Therefore, the usage of filters is important to filter out the unnecessary low energy of photon beam.

Meanwhile, the high energy of X-rays will penetrate through the patient body, and thus produce a series of raw projections data. The projection data at different angles is then reconstructed in a computer, and producing cross-sectional areas of the patient body. The image of cross-sectional areas is displayed and viewed in a computer, which is also function as storage of image data.

2.2.3 CT image formation

There are three phases in CT images formation; the scanning data phase, reconstruction phase and digital-to-analogue conversion phase as shown in Figure 2.7.

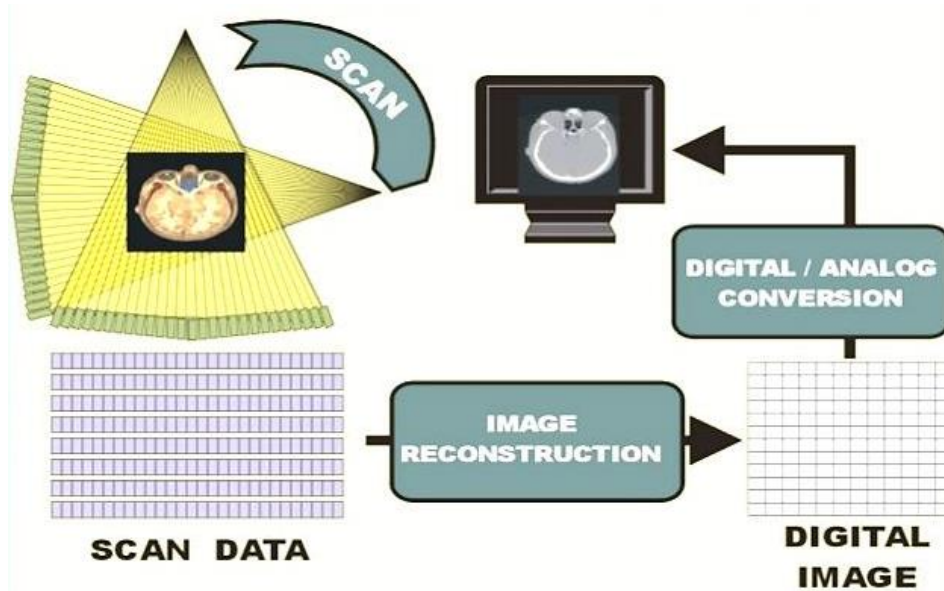


Figure 2.7. The phase of CT image formation; the scanning data phase, reconstruction phase and digital-to-analogue conversion phase (Sprawls, 1988).

2.2.3(a) Scanning phase

The scanning phase does not produce an image but they produce data. During this phase, a fan-shaped X-ray beam is rotated around the body to provide a cross-sectional image as shown in Figure 2.8. The attenuation measurement of each individual X-ray photon that transmitted through a body is recorded by the detectors. As the X-ray photon passes through the patients' body, total attenuation coefficient is measured and then is recorded by the detector.

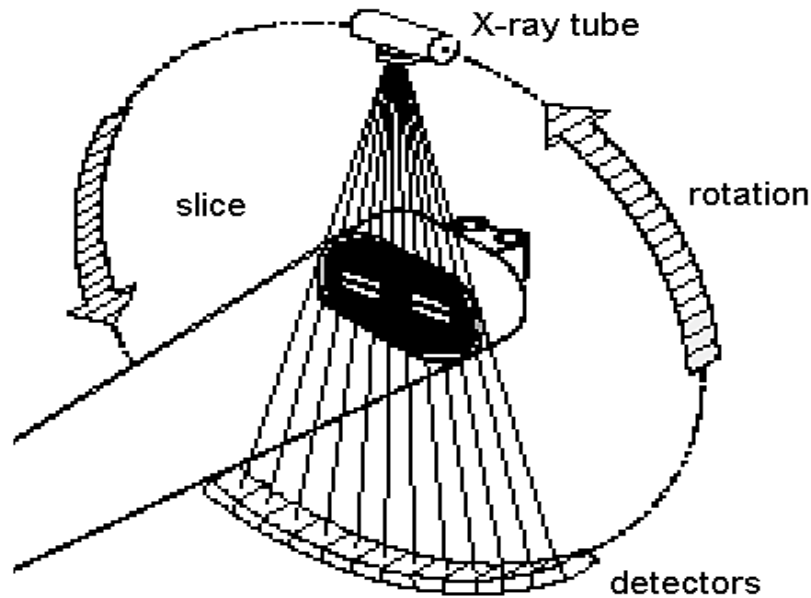


Figure 2.8. Diagram of CT scanning process which the patient is scanned with the X-ray source and detector rotates around the patient. Thin slice X-ray beams interact with the tissue and detector collect enough information from the interaction for image reconstruction (Illingworth, 2011).

As the X-ray photon passes through an object, the detectors detected the projected X-rays and measured the X-rays intensity. The intensity I is the sum of attenuation coefficients along the X-ray path. The attenuation of the incident photon depends on the incident photon energy and the atomic number of the absorbing material. The attenuation of X-ray photon occurs exponentially in the matter as the X-ray photons pass through and are shown in Equation 2.5.

2.2.3(b) Reconstruction phase

The projection data are then reconstructed by a method called back projection. Back projection is a process of tracing backwards the projection data along the X-rays forward path to reconstruct the image and calculating the absorption due to a localized region.